Title

Quantitative label-free digital holographic imaging of cardiomyocyte optical volume, nucleation, and cell division.

Authors

Huang, Herman
Park, Sangsoon
Ross, Ines
et al.

Publication Date

2024-11-01

DOI

10.1016/j.yjmcc.2024.09.003

Peer reviewed

HHS Public Access

Author manuscript

J Mol Cell Cardiol. Author manuscript; available in PMC 2025 February 06.

Published in final edited form as:

J Mol Cell Cardiol. 2024 November ; 196: 94–104. doi:10.1016/j.yjmcc.2024.09.003.

Quantitative Label-free Digital Holographic Imaging of Cardiomyocyte Optical Volume, Nucleation, and Cell Division

Herman Huang[4,*], **Sangsoon Park**[1,2,3,*], **Ines Ross**[4], **Joseph Moreno**[1,2,3], **Sheamin Khyeam**[1,2,3], **Jacquelyn Simmons**[4], **Guo N. Huang**[1,2,3,**], **Alexander Y. Payumo**[4,**]

[1]Cardiovascular Research Institute & Department of Physiology, University of California, San Francisco, San Francisco, CA, 94158, USA

[2]Eli and Edythe Broad Center for Regeneration Medicine and Stem Cell Research, University of California, San Francisco, San Francisco, CA, 94158, USA

[3]BAKAR Aging Research Institute, University of California, San Francisco, San Francisco, CA, 94158, USA

[4]Department of Biological Sciences, San Jose State University, San Jose, CA 95192, USA

Abstract

Cardiac regeneration in newborn rodents depends on the ability of pre-existing cardiomyocytes to proliferate and divide. This capacity is lost within the first week of postnatal development when these cells rapidly switch from hyperplasia to hypertrophy, withdraw from the cell cycle, become binucleated, and increase in size. How these dynamic changes in cell size and nucleation impact cardiomyocyte proliferative potential is not well understood. In this study, we innovate the application of a commercially available digital holographic imaging microscope, the Holomonitor M4, to evaluate the proliferative responses of mononucleated and binucleated cardiomyocytes after CHIR99021 treatment, a model proliferative stimulus. This system enables long-term label-free quantitative tracking of primary cardiomyocyte dynamics in real-time with single-cell resolution. Our results confirm that chemical inhibition of glycogen synthase kinase 3 with CHIR99021 promotes complete cell division of both mononucleated and binucleated cardiomyocytes with high frequency. Quantitative tracking of cardiomyocyte volume dynamics during these proliferative events revealed that both mononucleated and binucleated cardiomyocytes reach a similar size-increase threshold prior to attempted cell division. Binucleated cardiomyocytes attempt to divide with lower frequency than mononucleated cardiomyocytes, which may be associated with inadequate increases in cell size. By defining the interrelationship between cardiomyocyte size, nucleation, and cell cycle control, we may better

**co-correspondence: Guo.Huang@ucsf.edu; Alexander.Payumo@sjsu.edu.

*Equal contribution

AUTHOR CONTRIBUTIONS

HH, SP, GNH, and AYP designed experiments. HH, SP, IR, and AYP performed all experiments. HH, SP, IR, GNH, and AYP analyzed the data. JM, SK, and JS helped to optimize experimental conditions. HH, SP, GNH, and AYP drafted the manuscript. HH, SP, IR, JM, SK, JS, GNH, AYP edited and finalied the manuscript.

DISCLOSURES

None declared.

DECLARATION OF GENERATIVE AI AND AI-ASSISTED TECHNOLOGIES IN THE WRITING PROCESS

The authors did not use generative AI or AI-assisted technologies in the development of this manuscript.

understand the cellular mechanisms that drive the loss of mammalian cardiac regenerative capacity after birth.

Graphical Abstract:

Digital holographic imaging enables quantitative label-free three-dimensional tracking of cardiomyocyte and non-cardiomyocyte dynamics *in vitro*. Cardiomyocytes reach a size-increase threshold prior to cell division, which may be impaired by binucleation. Created with BioRender.com.

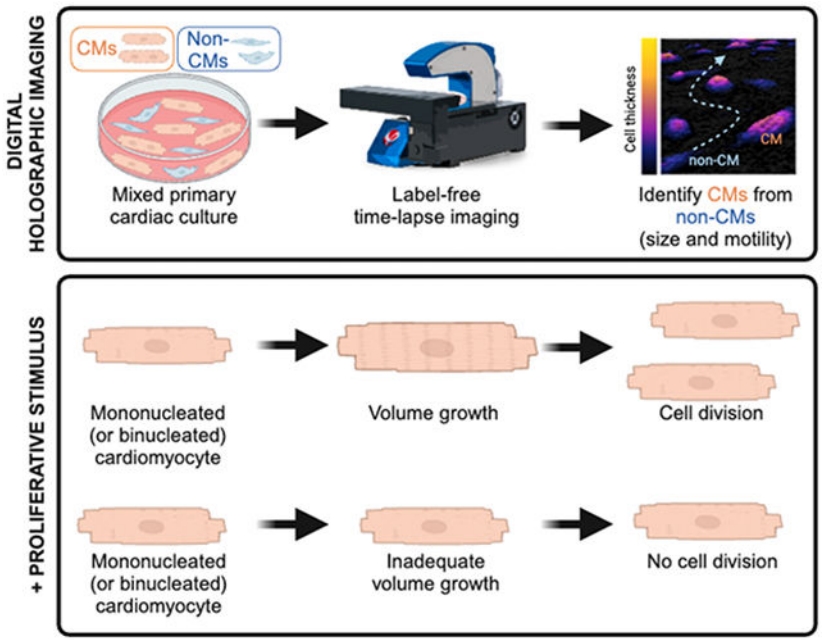

INTRODUCTION

Newborn rodents possess a transient capacity for cardiac regeneration that is lost shortly after birth (Porrello et al., 2011; H. Wang et al., 2020). Heart regeneration during this postnatal period relies on the ability of pre-existing cardiomyocytes to enter the cell cycle, divide, and replace damaged cardiac muscle tissue (Porrello et al., 2013). However, within this first week of life, rodent cardiomyocytes rapidly transition from hyperplasia to hypertrophy as they permanently withdraw from the cell cycle, undergo polyploidization, and increase in size (Bishop et al., 2021; Clubb & Bishop, 1984; Li et al., 1996; Soonpaa et al., 1996; Zak, 1973). During this transition, mononucleated diploid cardiomyocytes enter the cell cycle but fail to complete cytokinesis resulting in binucleated cells (Engel et al., 2006; Leone et al., 2018; Leone & Engel, 2019; Stopp et al., 2017). How increased cell size and nucleation impact cardiomyocyte cell cycle regulation and thus cardiac regenerative potential remains incompletely understood.

Cardiac primary cell culture represents a powerful *in vitro* approach to complement *in vivo* studies. Experiments using primary cardiomyocyte cultures from newborn rodents have revealed many intrinsic (e.g., transcription factors) and extrinsic (e.g., extracellular

matrix proteins, secreted factors) regulators of cardiomyocyte proliferation and hypertrophy (Mehdipour et al., 2023). Therefore, primary cardiac cell culture is a relevant approach to investigate questions regarding heart development, physiology, and pathophysiology, especially at the cellular and molecular levels.

A key challenge in studying cardiomyocyte cell cycle regulation is the difficulty to distinguish true cardiomyocyte cell division from cytokinesis failure and binucleation both *in vitro* and *in vivo* (Auchampach et al., 2022). Traditional approaches rely on tissue fixation and staining for commonly used cell cycle markers (e.g., Ki67, PHH3, AurkB, etc.) (Auchampach et al., 2022; Leone et al., 2015). However, the expression of these markers in cardiac muscle cells can often be misleading since they are similarly expressed in both cardiomyocytes that complete and fail cell division. Therefore, direct live-cell imaging of primary cardiomyocytes using phase contrast microscopy has been the most definitive approach to demonstrate true cardiomyocyte division and expansion *in vitro* (Leone et al., 2018; Leone & Engel, 2019; Yahalom-Ronen et al., 2015).

In this study, we innovate the application of a commercially available digital holographic phase imaging microscope, the HoloMonitor M4 (Phase Holographic Imaging; Lund, Sweden), to investigate how size and nucleation influence the outcomes of cardiomyocyte cell division *in vitro*. The Holomonitor M4 is fits within standard cell culture incubators and requires no additional environmental controllers for long-term imaging of living cells (Fig. 1A). The interference pattern created between a sample and reference beam generates phase shift data, which is then reconstructed to visualize the cultured cells in three dimensions (Fig. 1B).

This digital holographic imaging system has several advantages compared to existing live-cell imaging technologies (Mölder et al., 2008). First, imaging is performed with a low-power 635 nm laser, which minimizes phototoxicity to support long-term imaging of cellular behaviors. Second, full three-dimensional reconstructions are automatically generated for cells located within a 40 μm distance from the cell culture surface, which greatly ameliorates issues with maintaining sample focus during extended imaging durations. And third, the Holomonitor App Suite analysis software enables quantitative tracking of cell size, shape, and movement with single-cell resolution. Using this approach, we explore the interrelationship between cardiomyocyte size, nucleation, and cell cycle control to better understand the cellular mechanisms that drive the loss of mammalian cardiac regenerative capacity after birth.

RESULTS

Primary cardiomyocytes are distinguished from non-cardiomyocytes based on their larger size and limited motility

Primary rodent cardiomyocyte cultures derived from postnatal day 1 (P1) to P3 rats are often contaminated with non-cardiomyocytes including cardiac fibroblasts and endothelial cells. While methods to improve cardiomyocyte purity have been developed based on differential attachment speeds (Blondel et al., 1971) or densities (Sen et al., 1988), the addition of these enrichment steps nevertheless fail to completely remove all non-cardiomyocytes in the

culture. Therefore, live-imaging experiments of primary cardiac cultures often necessitates cardiomyocyte-specific labeling or post-imaging fixation and validation of cardiomyocyte identity by immunostaining, which adds to experimental complexity (Leone & Engel, 2021). Cardiomyocytes make up most of the heart's volume due to their larger size but are outnumbered by smaller cardiac fibroblasts and endothelial cells (Baum & Duffy, 2011). We therefore evaluated if our label-free digital holographic imaging approach could differentiate primary cardiomyocytes from non-cardiomyocytes in mixed cardiac cultures based on their unique three-dimensional morphologies and dynamics.

To define which primary cardiac cells observed on the Holomonitor M4 corresponded to cardiomyocytes, we first live-imaged the culture using digital holographic microscopy, fixed the cells, immunostained against the cardiomyocyte-specific marker α-actinin, and then re-imaged the same field by conventional fluorescence microscopy (Fig. 2A-B). The thicker and larger cells identified on the Holomonitor M4 most strongly correlated with α-actinin-positive cardiomyocytes (Fig. 2B-C). The maximum optical thickness (Fig. 2D) and optical volume (Fig. 2E) of these putative cardiomyocytes were 1.8-fold and 3.2-fold higher than non-cardiomyocytes, respectively. While size alone was a strong predictor of cardiomyocyte identity in most cases, we noticed a few thicker α-actinin-negative non-cardiomyocytes by digital holographic imaging at this time point (~7%) (Fig. 2A-B). However, we observed that non-cardiomyocyte thickness fluctuated over time and sharply increased prior to cell division (Movie S1). Therefore, to minimize misidentification of cardiomyocytes based on cell size analysis alone, we evaluated cellular motility as a secondary identification criterion and discovered that primary rat cardiomyocytes are slow moving, covering 6.7-fold less distance than non-cardiomyocytes within a 12-hour period (Fig. 2F-H; Movie S2). These data demonstrate that our label-free digital holographic imaging approach can reliably distinguish primary neonatal rat cardiomyocytes from non-cardiomyocytes based on their consistently larger size and limited motility (Supplementary Methods). We additionally found that these criteria can be similarly applied to identify primary mouse cardiomyocytes as well (Fig. S1), broadening the applicability of this approach.

Digital holographic imaging permits quantitative tracking of cardiomyocyte optical volume dynamics with single-cell resolution

Cardiomyocytes undergo hypertrophy to maintain cardiovascular function in response to overload (Nakamura & Sadoshima, 2018), and this response can be modeled *in vitro*. For example, treatment of cultured primary rat cardiomyocytes with the sympathetic neurohormone norepinephrine results in hypertrophic growth through activation of α_1-adrenergic receptors (Simpson, 1985). Phenylephrine is a selective α_1-adrenergic receptor agonist that promotes cardiomyocyte hypertrophy by inducing protein synthesis via various pathways including MAPK/ERK (Rolfe et al., 2005) and mTOR signaling (Hannan et al., 2003). We thus evaluated the quantitative capacities of the HoloMonitor M4 to detect changes in three-dimensional cardiomyocyte volume after stimulation with phenylephrine.

Treatment with 50 μM phenylephrine for 48 hours increased the two-dimensional size of α-actinin-positive cardiomyocytes as visualized by conventional fluorescence imaging (Fig. 3A-B). We next employed our digital holographic imaging approach to quantify the

three-dimensional optical volumes of individual cardiomyocytes prior to and after 48-hour treatment with phenylephrine (Fig. 3C-F). While no significant differences were observed in the optical volumes between untreated (n = 305) and treated (n = 300) cardiomyocytes at the start of the experiment (Fig. 3D), the average optical volume increased by 1.33-fold in treated cells after 48 hours (Fig. 3E; Movie S3).

Single-cardiomyocyte tracking revealed heterogeneity in cardiomyocyte volume responses to the hypertrophic stimulus (Fig. 3F). For example, 48.2% of untreated cardiomyocytes decreased in volume over the 48-hour period in comparison to only 13% of cardiomyocytes stimulated with phenylephrine. 50.8% of untreated cardiomyocytes demonstrated a modest less than two-fold increase in optical volume while 75.3%, 9.3%, and 1.3% of phenylephrine-treated cardiomyocytes exhibited a wider range in cell growth between 1- and 2-fold, 2- and 3-fold, and greater than 3-fold, respectively (Fig. 3G). These experiments validate our approach to dynamically track optical volume changes in individual primary cardiomyocytes over time.

Cardiomyocytes stimulated with CHIR99021 undergo both successful and failed attempts at cell division

In our base serum-free culture conditions, we evaluated the frequency of cardiomyocyte cell cycle entry by incubating primary neonatal rat cardiomyocytes in the thymidine analog 5-ethynyl-2'deoxyridine (EdU) for 48 hours, which marks cells undergoing DNA synthesis (S-phase) within that time period. After immunostaining against the cardiomyocyte-specific marker cardiac troponin T (cTnT), we quantified the percentage of cardiomyocytes that incorporated EdU and determined that only 8.37% of these cells had entered S-phase (Fig. 4A, 4C). Tracking of 301 randomly chosen cardiomyocytes using our digital holographic imaging approach revealed that only 6 (2%) of cardiomyocytes were able to divide under our base culture conditions (Fig. 4F; Movie S4). Because this low frequency of cardiomyocyte cell cycle entry would be challenging to monitor in our label-free digital holographic imaging experiments, we sought ways to better support robust cardiomyocyte proliferation *in vitro* while maintaining chemically-defined conditions.

Glycogen synthase kinase 3 (Gsk3) has been proposed as a therapeutic target for cardiac regenerative medicine (Singh et al., 2019). Treatment of primary neonatal rat cardiomyocytes with the Gsk3 inhibitor 6-bromoindirubin-30-oxime (BIO) resulted in a 10-fold increase in cardiomyocyte cell cycle entry (Tseng et al., 2006). More recently, the Gsk3β-specific inhibitor CHIR99021 was discovered to increase the expression of cell cycle markers in primary cultured neonatal human atrial cardiomyocytes through activation of Wnt/β-catenin signaling (Ring et al., 2003; S. Wang et al., 2016). *In vivo*, tamoxifen-induced cardiomyocyte-specific combinatorial knockouts of both Gsk3α and Gsk3β in adult mouse hearts increased cardiomyocyte cell cycle activity and promoted further multinucleation, but resulted in mitotic catastrophe and apoptosis (Zhou et al., 2016). Therefore, we reasoned that chemical inhibition of Gsk3 would be a therapeutically relevant model stimulus to evaluate cardiomyocyte proliferative responses in our *in vitro* system to discover aspects of postnatal cardiomyocyte maturation that may impair cell division.

Treatment of primary cardiac cultures with 5 μM CHIR99021 robustly increased cardiomyocyte-specific EdU incorporation to 84.0%, a 10-fold increase above that observed using our base media alone (Fig. 4B, 4C). During these 48 hours of continuous stimulation with CHIR99021, digital holographic imaging revealed dramatic changes in cardiomyocyte morphology and behavior (Fig. 4D; Movie S4), including notable increases in cardiomyocyte size. We quantified the single-cell behaviors of 485 randomly chosen cardiomyocytes to further understand their individual responses to the defined proliferative stimulus. We observed cardiomyocytes that 1) completed cell division, 2) failed cell division, or 3) made no attempt at cell division within the 48-hour experimental window (Fig. 4E; Supplementary Methods). We examined the frequencies of these major outcomes and discovered that 58.8% (285/485) of cardiomyocytes analyzed displayed complete cell division while 15.9% (77/485) failed to completely divide, which suggests that 74.7% (362/485) of all cardiomyocytes analyzed had entered the cell cycle. This overall frequency of cardiomyocyte cell cycle entry after treatment with CHIR99021 is in agreement with that predicted by our post-fixation EdU staining experiments (Fig. 4C).

Binucleated cardiomyocytes exhibit a blunted proliferative response but retain significant capacity for successful cell division

We noticed that it was possible to distinguish mononucleated from binucleated cardiomyocytes by identifying their nuclei based on their differential densities when compared to that of the surrounding perinuclear regions (Fig. 5A; Supplementary Methods). During our digital holographic imaging experiments, cardiomyocyte nuclei could be identified as round structures with approximately 10 μm diameters that exhibit less overall vertical thickness. Binucleation is thought to limit the proliferative potential of cardiomyocytes and is considered a major barrier to cardiac regeneration (Derks & Bergmann, 2020; Huang et al., 2023; Mehdipour et al., 2023). Therefore, we next determined if mononucleated and binucleated cardiomyocytes exhibited different proliferative responses to CHIR99021 stimulation.

We subcategorized the 485 CHIR99021-stimulated cardiomyocytes analyzed previously (Fig. 4F) into mononucleated (n = 373, 76.9%) and binucleated (n = 112, 23.1%) cells. These primary cardiac cultures were derived from postnatal day 3 (P3) neonatal rats, a developmental stage when cardiomyocytes are just beginning to binucleate *in vivo* (Li et al., 1996). Since our cultures contain a mixture of both mononucleated and recently binucleated cardiomyocytes derived from the same hearts, we are able to more directly resolve the unique behaviors of these cells under identical culture conditions without any further experimental manipulation. In response to 5 μM CHIR99021 treatment for 48 hours, we observed subpopulations of both mononucleated and binucleated cardiomyocytes attempting to divide. Strikingly, all observed events began with the cardiomyocyte rounding and increasing in thickness while maintaining attachment to the substratum within 20 minutes of attempted division (Fig. 5A), regardless of nuclei number. Mitotic rounding enabled by compliant extracellular matrices has been positively associated with complete cardiomyocyte cell division (Yahalom-Ronen et al., 2015). However, a recent report suggests that rounding is not a marker to discriminate between complete cardiomyocyte division and binucleation (Leone et al., 2018). Our findings are consistent with the latter study and

support that mitotic rounding itself is not a sufficient marker to predict true cardiomyocyte cell division.

Despite our observation that all cardiomyocytes analyzed rounded prior to attempted cell division, not all cells were able to divide successfully. Cardiomyocytes that successfully divided initiated mitotic rounding, separated into two distinct cells, which remained separated. Cardiomyocytes that failed to divide initiated mitotic rounding, attempted to separate into two distinct cells, but immediately snapped back together (Supplementary Methods). These dynamics could be readily observed in our holographic imaging time-lapse movies (Movies S5-6). 81.5% (304/373) of all mononucleated cardiomyocytes analyzed attempted to divide, with the majority, 78.3% (238/304), successfully completing cell division and 21.7% (66/304) failing to completely separate (Fig. 5B; Movie S5). We were able to observe the resulting nucleation state of 55 mononucleated cardiomyocytes that failed to divide and found that 100% (55/55) became binucleated, consistent with failed cytokinesis. Overall, these findings are consistent with previous observations that mononucleated cardiomyocytes retain high proliferative and regenerative potential (Becker & Hesse, 2020; Leone et al., 2018). In contrast, 51.8% (58/112) of all binucleated cardiomyocytes analyzed attempted to divide with 81.0% (48/58) successfully completing cell division and 19.0% (11/58) failing cytokinesis (Fig. 5B; Movie S6). We were only able to observe the resulting nucleation state of 4 binucleated cardiomyocytes that failed to divide and found that they remained binucleated. Since our approach cannot measure DNA content, it remains unclear if the resulting nuclei are polyploid. These results suggest that binucleation may blunt a cardiomyocyte's ability to attempt cell division in response to a proliferative stimulus, but not significantly impact the success rate of division. This is in agreement with previous work documenting the successful division of binucleated rat cardiomyocytes *in vitro*, which may occur through the formation of pseudo-bipolar mitotic spindles (D'Uva et al., 2015; Leone & Engel, 2019; W. E. Wang et al., 2017).

Mononucleated and binucleated cardiomyocytes reach a similar size-increase threshold prior to attempted cell division

While only 18.5% (69/373) of mononucleated cardiomyocytes did not attempt cell division in response to 5 μM CHIR99021 stimulation, the 48.2% (54/112) of binucleated cells analyzed made no attempt to do so (Fig. 5B). Previous studies have proposed that mammalian cells may need to meet a critical size threshold in order to exit from the G1 phase, progress through the cell cycle, and divide (Ginzberg et al., 2015). Increased DNA content is generally associated with increased cell size (Amodeo & Skotheim, 2016), and binucleated cardiomyocytes are noticeably larger than mononucleated cardiomyocytes (Windmueller et al., 2020). We wondered if cardiomyocytes that did not attempt to divide in response to CHIR99021 treatment failed to reach a critical size-increase threshold to progress through the cell cycle. Therefore, we determined if such a size-increase threshold exists in primary cardiomyocytes prior to attempted cell division and how binucleation influences this parameter.

We applied our digital holographic imaging approach to assess cell volume changes during the proliferative responses of both mononucleated and binucleated cardiomyocytes. We

measured the initial optical volumes of P3 mononucleated and binucleated cardiomyocytes at the time of CHIR99021 stimulation. The average optical volumes of mononucleated and binucleated cardiomyocytes were 1400 +/− 361 μm^3 and 2201 +/− 676 μm^3, respectively (Fig. 5C), confirming that binucleated cardiomyocytes are initially larger than mononucleated cardiomyocytes. These volume measurements are inline with those previously estimated by Coulter counter analysis (Li et al., 1996). To determine the size of these same cells just prior to cell division, we measured cardiomyocyte optical volumes at the time of rounding (Fig. 5D). The average optical volumes of mononucleated and binucleated cardiomyocytes at rounding were 2875 +/− 708 μm^3 and 4578 +/− 1246 μm^3, respectively. However, when evaluating the overall ratios by which these cells increased their volumes prior to attempted cell division, we noted that mononucleated and binucleated cardiomyocytes similarly enlarged by 2.18 +/− 0.76-fold and 2.15 +/− 0.66-fold, respectively (Fig. 5E). The volumes of the daughter cells resulting from complete mononucleated or binucleated cardiomyocyte cell division were similar to volumes of the parent cardiomyocytes at the start of the imaging experiment (Fig. S2). Additionally, we observed that mononucleated cardiomyocytes that failed to divide tended to be slightly larger than those that completed cell division at the start of our imaging experiments (Fig. S3). Taken together, these results demonstrate that while binucleation increases the absolute size of cardiomyocyte, it does not alter the relative size-increase threshold that may be required for attempted cell division.

We then further analyzed the individual responses of cardiomyocytes that made no attempt to divide despite stimulation with CHIR99021. The 69 mononucleated and 54 binucleated cardiomyocytes that did not attempt cell division within 48 hours increased in volume by only 1.79 +/− 0.78-fold and 1.76 +/− 0.6-fold on average, respectively, by the end of our video recordings (Fig. 5E). These findings suggest that mononucleated and binucleated cardiomyocytes that fail to meet the size-increase threshold in response to CHIR99021 may not attempt to divide.

The timing of attempted cell division is slightly delayed in binucleated cardiomyocytes

We evaluated the timing of cardiomyocyte attempted cell division after stimulation with 5 μM CHIR99021 (Fig. S4). Mononucleated cardiomyocytes that attempted to divide did so within 1740 +/− 381 minutes. Binucleated cardiomyocytes exhibited a slight delay and attempted to divide within 1906 +/− 480 minutes. We also observed a slight inverse relationship between initial cell volume and the timing of attempted cell division in mononucleated but not binucleated cardiomyocytes (Fig. S4B-C). In our experiments, all cardiomyocytes analyzed attempted to divide within 29-32 hours on average in response to CHIR99021 treatment. This is in line with a previous *ex vivo* imaging study estimating the total cell cycle length of ventricular cardiomyocytes to be around 30-35 hours (Hashimoto et al., 2014).

DISCUSSION

As the advantages of digital holographic imaging are gradually being recognized, multiple applications of the Holomonitor M4 have recently been reported in various contexts such as

wound healing, cell motility, three-dimensional culture of cells in matrigel, and optogenetics (Fang et al., 2023; Hellesvik et al., 2020; Tahara et al., 2018; Zhang & Judson, 2018). However, the application of digital holographic imaging in cardiovascular research has thus far been limited. The versatility of this instrument may have great potential to increase our cellular understanding of cardiomyocyte hypertrophy, migration, response to ischemia-reperfusion, and intercellular interactions. We've recently shown the utility of this approach to monitor longitudinal cardiomyocyte hypertrophic growth dynamics in response to catecholamine stimulation (Akter et al., 2024).

Previous methods to directly evaluate cardiomyocyte size each have unique experimental limitations. For example, two-dimensional cardiomyocyte surface area measurements (Watkins et al., 2012) fail to consider changes in cell thickness and more directly evaluate cell spreading. Coulter counters (Li et al., 1996) and flow cytometry (Nakano et al., 2017) provide population-based measurements but do not resolve single-cell dynamics. And three-dimensional confocal imaging (Satoh et al., 1996) typically requires cell fixation and optical sectioning with high-powered lasers thus limiting long-term imaging of living cardiomyocytes.

In this study, we demonstrate that digital holographic imaging circumvents many of the limitations listed above and is a powerful methodology to quantitatively track primary cardiomyocyte size, nucleation, and cell division in real-time with single-cell resolution. In rodents, mononucleated diploid cardiomyocytes attempt to divide, but fail cytokinesis, become binucleated, undergo cell cycle arrest, and increase in size within the first weeks of postnatal development (Bishop et al., 2021; Clubb & Bishop, 1984; Li et al., 1996; Soonpaa et al., 1996; Zak, 1973). The interplay between cardiomyocyte size, nucleation state, and cell cycle regulation during this developmental transition is not well understood. Therefore, our unique application of digital holographic imaging technology is relevant to understanding the cellular mechanisms by which mammalian hearts lose their capacity for heart regeneration shortly after birth.

Our studies are the first to demonstrate that both mononucleated and binucleated cardiomyocytes increase similarly in volume — 2.18-fold and 2.14-fold, respectively — prior to attempting cell division (Fig. 5E). Importantly, while the relative increase in size is conserved, binucleation increases the absolute volume of this threshold (Fig. 5D). This suggests that DNA copy number itself may directly regulate size dynamics in cycling cardiomyocytes. Cell growth has recently been reported to play an important role in cell cycle regulation by diluting the concentration of cell cycle inhibitors to trigger progression through the G1-S transition (Zatulovskiy et al., 2020). It is possible that an increased copy number of genes encoding cell cycle inhibitors requires compensatory increases in cell volume in order to dilute inhibitor concentrations and permit cell division in binucleated cardiomyocytes. Unlike adult rodent cardiomyocytes that are mostly binucleated, the majority of adult human cardiomyocytes are mononucleated and polyploid due to defects in nuclear division (Derks & Bergmann, 2020). It remains to be determined how size may influence nuclear or cytoplasmic separation in human or rodent cardiomyocytes, respectively.

Finally, we observed that 63.8% of mononucleated and 42.0% of binucleated cardiomyocytes analyzed successfully divided (Fig. 5B). These results are aligned with previous observations that binucleated cardiomyocytes retain potential for successful cell division *in vitro* (Leone & Engel, 2019). Non-responsive cardiomyocytes regardless of nucleation state exhibited a statistically significant deficiency in growth during our 48-hour imaging experiments (Fig. 5E), which may suggest that cardiomyocytes must reach a size-increase threshold to attempt cell division. However, the results from a recent study using Mosaic Analysis with Double Markers (MADM) mice to demonstrate true adult cardiomyocyte cell division *in vivo* indicate that newly generated daughters may actually be smaller in size than unstimulated control cardiomyocytes (Mohamed et al., 2018). This would suggest that adult mouse cardiomyocytes undergo volume reduction rather than increase in size prior to successful cell division. Transgenic mice with cardiomyocyte-specific expression of the fluorescence ubiquitination cell cycle indicator (FUCCI) show that adult mouse cardiomyocytes may be arrested in the G1-S cell cycle transition (Alvarez et al., 2019). The G1 phase is typically associated with cell growth (Zatulovskiy et al., 2020). Therefore, one possible interpretation is that adult cardiomyocytes are already stalled at a permissive size for cell division, but fail to progress through the G1-S transition due to other inhibitory mechanisms. While the experiments performed in this study focused on early neonatal cardiomyocytes from P1 to P3 rat pups, it may be possible to also apply this technology to evaluate how cardiomyocytes isolated from more mature hearts (P8+) respond to proliferative stimuli. Future work to better understand the interrelationship between cardiomyocyte size and cell cycle progression will be necessary to inform new strategies in cardiac regenerative medicine to trigger successful cell division in adult mammalian heart muscle cells.

While we demonstrate the capabilities of the Holomonitor M4 digital holographic microscope in our study, we also note the technical limitations of the technology. For example, when measuring cellular optical volumes, the Holomonitor M4 and analysis software must identify true signal from background noise and there is some associated error in that measurement. This error is likely enhanced when evaluating smaller, thinner cells that tend to spread out on the cell culture surface (e.g., fibroblasts). Fortunately, primary cardiomyocytes tend to be larger, thicker cells (Fig. 2B-C), which lessens the impact of this error in our measurements. Another limitation is that the image segmentation and cell tracking features in the Holomonitor App Suite software does not perform well when cells are clustered very closely together. Therefore, to maintain the accuracy of our measurements, we focused our single-cell tracking to well-isolated cardiomyocytes not integrated within tight clusters. This requirement would not be compatible with studies seeking to investigate cellular functions in the context of complex multicellular tissue environments. Additionally, defining the nucleation state of cardiomyocytes based on the differences in optical thickness between nuclei and the surrounding cytoplasm is not ideal. We find that the visibility of cardiomyocyte nuclei isn’t always apparent and may be dependent on culture conditions (Supplementary Methods). We acknowledge that our label-free digital holographic imaging approach does not formally distinguish changes in DNA ploidy; therefore, cardiomyocytes that may undergo DNA replication without nuclear division (i.e., endomitosis) are not identified. Finally, it is important to clarify that the

cardiomyocyte proliferative dynamics we observe in this study are specific to CHIR99021 stimulation under our culture conditions. It remains possible that alternate behaviors can be observed if cardiomyocytes are triggered to divide using other stimuli (e.g., fetal bovine serum). Nevertheless, our studies provide an example of how digital holographic microscopy can be leveraged to further understand the intrinsic cellular mechanisms that regulate cardiomyocyte proliferative potential.

MATERIALS AND METHODS

Animal breeding

Neonatal rat and mouse pups were generated through natural matings approved by Institutional Animal Care and Use Committee (IACUC) protocols 1072 (Dr. Payumo, San Jose State University) and AN197871–00B (Dr. Huang, University of California, San Francisco).

Cardiomyocyte isolation and culture

Postnatal day 1 (P1) to P3 Sprague Dawley rat pups were euthanized by decapitation under manual restraint. Hearts were harvested and the aorta was pinched closed with forceps. The coronary vessels were then reverse-perfused with cardiomyocyte isolation buffer (CIB; 120 mM sodium chloride, 15 mM potassium chloride, 0.6 mM monopotassium phosphate, 0.6 mM sodium phosphate dibasic heptahydrate, 1.2 mM magnesium sulfate heptahydrate, 10 mM HEPES, 4.6 mM sodium bicarbonate, 30 mM taurine, 10 mM 2,3-butanedione monoxime, 5.5 mM glucose) supplemented with 0.4 mM EGTA by inserting a 20G needle into the left ventricle to clear out blood and improve digestion efficiency. After perfusion, the ventricles were isolated, cut into pieces, and transferred into a digestion buffer consisting of 2 mg/mL collagenase II (LS004176, Worthington Biochemical) and 0.3 mM calcium chloride in CIB. Tissues were digested at 37°C under gentle agitation for approximately 2 hours while collecting dissociated cells every 15 to 30 minutes until complete digestion. Collections were pooled and stored on ice to limit collagenase activity. After digestion, the dissociated cells were gently centrifuged for 5 minutes at 200 x g, resuspended in wash buffer 1 (CIB, 10% FBS, 0.64 mM calcium chloride), again in wash buffer 2 (CIB, 10% FBS, 1mM calcium chloride), and then in plating media composed of 10% FBS in DMEM/F12 (SH30023.01, Cytiva) with 100 μg/mL Primocin (ant-pm, InvivoGen). Cells were then passed through a 70-μm cell strainer (258368, Nest Scientific, NJ, USA) into a 6-well plate for pre-plating at 37°C in a 5% CO_2 incubator for 1 to 2 hours to deplete non-cardiomyocyte populations via differential attachment. After pre-plating, the media and remaining cells were collected, quantified, and then seeded into 6-well plates (800,000 cells per well) or 12-well plates (400,000 cells per well) coated with 1% w/v gelatin (G9391, Sigma-Aldrich) in plating media overnight to allow cardiomyocyte attachment.

Neonatal mouse cardiomyocytes from ICR pups were isolated similarly with the following modifications. The digestion buffer additionally contained 0.2 mg/mL protease type XIV (P5147, Sigma-Aldrich), which may further help dissociate cell clusters into single cardiomyocytes. Also, 10% FBS was added prior to pooling each collection during digestion on ice to further protect the dissociated cells. Finally, after the preplating step, the

cardiomyocyte-enriched cells were seeded into 96-well plates coated with 5 ug/cm^2 rat tail collagen I (354236, Corning) in plating media at a density of 80,000-150,000 cells per well.

Chemical treatments

Freshly isolated cardiac cells were cultured in plating media for 16-24 hours to allow attachment to the culture vessel. The next day, the cells were washed briefly three times in PBS to remove serum and then switched to a serum-free culture media composed of DMEM/F12 supplemented with 1X insulin, transferrin, and selenium (ITS, 400-145, GeminiBio) and 100 μg/mL primocin. At this time, cultures were additionally treated with 50 μM phenylephrine (P6126, Sigma-Alrdich) or 5 μM CHIR99021 (A133052, Ambeed) for 48 hours under serum-free conditions to stimulate cardiomyocyte hypertrophy or proliferation, respectively. When specified, cells were also incubated in 5 μM 5-ethynyl-2′-deoxyuridine (EdU, NE08701, Biosynth) for 48 hours to incorporate this thymidine analogue in any cell undergoing DNA synthesis within the treatment period.

EdU detection

After chemical treatments, cardiac cultures were fixed in 10% formalin (15740-01, Electron Microscopy Sciences) for 15 minutes at room temperature. To detect EdU incorporation, cells were washed three times with PBS and blocked with 3% bovine serum albumin (A8412, Sigma-Aldrich) in PBS for 30 minutes at room temperature. Click chemistry was then performed to covalently attach an azide-containing fluorescent dye to the alkyne group available on EdU. In short, cells were treated with 10 μM FAM azide 6-isomer (A5130, Lumiprobe) in the presence of 1 mM $CuSO_4$ and 250 μM ascorbic acid (AO537, Tokyo Chemical Industry) in 100 mM Tris pH 8.0 (AO321, Tokyo Chemical Industry) for 30 minutes.

Immunohistochemistry

For rat cardiac cultures, samples were washed three times with 0.2% Triton X-100 in PBS (PBST) and then blocked in 10% FBS in PBST for 1 hour at room temperature directly after fixation or EdU detection. Cells were then incubated in cardiac troponin T antibody (MS-295-P1, Epredia) diluted 1:400 in PBST or alpha-actinin antibody (MA1-22863, Invitrogen) diluted 1:200 in PBST overnight at 4°C. The samples were again washed three times in PBST and then incubated in either Alexa Fluor 555 anti-mouse (A-31570, Thermo Fisher Scientific) or Alexa Fluor 488 anti-rabbit (711-545-152, Jackson ImmunoResearch) secondary antibodies diluted 1:500 in PBST for two hours at room temperature. Afterwards, the samples were washed three times in PBST with the first wash containing 1 μg/mL 4', 6-diamidino-2-phenylindole (DAPI, AB2285492, Abcam) in order to stain nuclei prior to imaging on a Keyence BZ-X810 or Nikon TE300 inverted microscopes.

Mouse cardiac cultures were stained as above with the following modifications. Fixed cells were blocked in 5% normal donkey serum (NC9624464, Jackson ImmunoResearch) in PBST for 1 hour at room temperature prior to incubation in cardiac troponin T antibody. Nuclei were instead stained with 10 μg/mL Hoechst 33342 (5117, Tocris Bioscience) in the final washes of the protocol prior to imaging on a Nikon Eclipse Ti inverted microscope.

Digital holographic time-lapse imaging

The Holomonitor M4 digital holographic microscope was purchased from Phase Holographic Imaging (PHI, Sweden) and placed directly within a Heracell 150 CO_2 incubator (Thermo Scientific). All connecting cables between the microscope and computer were routed through the door seals. For digital holographic imaging experiments, rat cardiac cells were cultured and treated with chemicals in 6-well plates (83.3920, Sarstedt) and then covered with HoloLids (PHI, Sweden) to stabilize imaging conditions. The cultures were then transferred into a 37°C to acclimate for an additional 1 hour and reduce condensation on the well bottoms. 10 imaging positions were then selected per treatment using the HOLOMONITOR App Suite software. This process took approximately 30 minutes. Live rat cardiac cultures were imaged on the Holomonitor M4 for 48 to 72 hours with time points taken every 20 min at 37°C and 5% CO_2.

Mouse cardiac cells were cultured in a 96-well plate (83.3924, Sarstedt) for 2 days in plating media to allow attachment. Cells were then switched to a serum-free media composed of MCDB107 (E3000, United States Biological), 1X ITS (I3146, Sigma-Aldrich) and 100 μg/mL of Primocin. Prior to imaging on the Holomonitor M4, the plate was covered with HoloLids and images were acquired every hour for 5 days at 37°C and 5% CO_2.

Quantitative cell size and motility analyses

Time-lapse recordings were analyzed in the Holomonitor App Suite software (PHI, Sweden) using the “In-depth Analysis: Single Cell Tracking” feature to segment, trace, and quantify single cell dynamics. The following segmentation thresholds were applied to generate the results shown in Figures 2, 3, and Supplementary Figure 1: auto-minimum error method, adjustment 128, minimum object size 20. The following segmentation thresholds were applied to generate the results shown in Figures 4, 5, and Supplementary Figure 2: auto-minimum error method, adjustment 131, minimum object size 18. Cardiomyocytes were qualitatively distinguished from non-cardiomyocytes based on their larger size and limited motility as shown in Figure 2. The Holomonitor App Suite software was then used to track individual cells and optical volume, thickness, and motility measurements were taken at the specified time points. Care was taken to ensure that all cells analyzed were well-isolated and the accuracy of cell segmentation was manually verified on each imaging frame. Cardiomyocyte optical volume measurements shown in Figures 4 and 5 are presented per each replicate isolation (Table S1).

Cardiomyocyte cell division analysis

72-hour time-lapse recordings were taken after stimulating the cardiac cultures to proliferate with CHIR99021. These recordings were analyzed in the Holomonitor App Suite software and well-isolated cardiomyocytes were identified and tracked using the “In-depth Analysis: Single Cell Tracking” feature. Mononucleated and binucleated cardiomyocytes were distinguished based on the number of visible nuclei identified within the cell. Within a 48-hour evaluation period, cardiomyocytes exhibiting complete furrow formation and separation into distinct daughter cells were considered to completely divide. Cardiomyocytes that attempted to separate but failed to resolve into two independent daughter cells were considered to incompletely divide. Cardiomyocytes that did not exhibit

mitotic rounding during the 48-hour evaluation period were considered to have made no attempt at cell division. The extra 24 hours of the 72 hour time-lapse recordings was used to clarify cell division outcomes if necessary. Cardiomyocyte cell division outcomes shown in Figures 4 and 5 are presented per each replicate isolation (Table S1).

Statistical analysis

All statistical analyses were performed using the GraphPad Prism software (GraphPad Software Inc.). Specific details including the statistical tests performed and the number of samples analyzed are reported in the corresponding figure legends.

Supplementary Material

Refer to Web version on PubMed Central for supplementary material.

ACKNOWLEDGEMENTS

We thank Huang and Payumo laboratory members for their valuable advice on the manuscript. We thank Dr. Kersti Alm of Phase Holographic Imaging for technical advice.

FUNDING

This work was supported by an American Heart Association Postdoctoral Fellowship [https://doi.org/10.58275/AHA.23POST1011296.pc.gr.161362 to S. Park; NIH awards [R01HL138456, R01HL157280], American Heart Association Transformation Award and Established Investigator Award, and Tobacco-Related Disease Research Program Award [P0558275] to Dr. G. N. Huang; and an NIH SuRE-First award [R16GM146643] to Dr. A. Y. Payumo.

DATA AVAILABILITY STATEMENT

The data underlying this article are available in the article and in its online supplementary material.

REFERENCES

Akter W, Huang H, Simmons J, & Payumo AY (2024). Application of Digital Holographic Imaging to Monitor Real-Time Cardiomyocyte Hypertrophy Dynamics in Response to Norepinephrine Stimulation. Applied Sciences (Basel, Switzerland), 14(9), 3819. 10.3390/app14093819 [PubMed: 38818302]

Alvarez R, Wang BJ, Quijada PJ, Avitabile D, Ho T, Shaitrit M, Chavarria M, Firouzi F, Ebeid D, Monsanto MM, Navarrete N, Moshref M, Siddiqi S, Broughton KM, Bailey BA, Gude NA, & Sussman MA (2019). Cardiomyocyte cell cycle dynamics and proliferation revealed through cardiac-specific transgenesis of fluorescent ubiquitinated cell cycle indicator (FUCCI). Journal of Molecular and Cellular Cardiology, 127, 154–164. 10.1016/j.yjmcc.2018.12.007 [PubMed: 30571978]

Amodeo AA, & Skotheim JM (2016). Cell-Size Control. Cold Spring Harbor Perspectives in Biology, 8(4), a019083. 10.1101/cshperspect.a019083 [PubMed: 26254313]

Auchampach J, Han L, Huang GN, Kühn B, Lough JW, O'Meara CC, Payumo AY, Rosenthal NA, Sucov HM, Yutzey KE, & Patterson M (2022). Measuring cardiomyocyte cell-cycle activity and proliferation in the age of heart regeneration. American Journal of Physiology. Heart and Circulatory Physiology, 322(4), H579–H596. 10.1152/ajpheart.00666.2021 [PubMed: 35179974]

Baum J, & Duffy HS (2011). Fibroblasts and Myofibroblasts: What are we talking about? Journal of Cardiovascular Pharmacology, 57(4), 376–379. 10.1097/FJC.0b013e3182116e39 [PubMed: 21297493]

Becker C, & Hesse M (2020). Role of Mononuclear Cardiomyocytes in Cardiac Turnover and Regeneration. Current Cardiology Reports, 22(6), 39. 10.1007/s11886-020-01289-y [PubMed: 32430578]

Bishop SP, Zhou Y, Nakada Y, & Zhang J (2021). Changes in Cardiomyocyte Cell Cycle and Hypertrophic Growth During Fetal to Adult in Mammals. Journal of the American Heart Association, 10(2), e017839. 10.1161/JAHA.120.017839 [PubMed: 33399005]

Blondel B, Roijen I, & Cheneval JP (1971). Heart cells in culture: A simple method for increasing the proportion of myoblasts. Experientia, 27(3), 356–358. 10.1007/BF02138197 [PubMed: 5546673]

Clubb FJ, & Bishop SP (1984). Formation of binucleated myocardial cells in the neonatal rat. An index for growth hypertrophy. Laboratory Investigation; a Journal of Technical Methods and Pathology, 50(5), 571–577. [PubMed: 6232423]

Derks W, & Bergmann O (2020). Polyploidy in Cardiomyocytes: Roadblock to Heart Regeneration? Circulation Research, 126(4), 552–565. 10.1161/CIRCRESAHA.119.315408 [PubMed: 32078450]

D'Uva G, Aharonov A, Lauriola M, Kain D, Yahalom-Ronen Y, Carvalho S, Weisinger K, Bassat E, Rajchman D, Yifa O, Lysenko M, Konfino T, Hegesh J, Brenner O, Neeman M, Yarden Y, Leor J, Sarig R, Harvey RP, & Tzahor E (2015). ERBB2 triggers mammalian heart regeneration by promoting cardiomyocyte dedifferentiation and proliferation. Nature Cell Biology, 17(5), Article 5. 10.1038/ncb3149 [PubMed: 25679030]

Engel FB, Schebesta M, & Keating MT (2006). Anillin localization defect in cardiomyocyte binucleation. Journal of Molecular and Cellular Cardiology, 41(4), 601–612. 10.1016/j.yjmcc.2006.06.012 [PubMed: 16889791]

Fang L, Li Z, Yu B, & Zhou L (2023). FGF23 promotes proliferation, migration and invasion by regulating miR-340-5p in osteosarcoma. Journal of Orthopaedic Surgery and Research, 18, 12. 10.1186/s13018-022-03483-w [PubMed: 36604721]

Ginzberg MB, Kafri R, & Kirschner M (2015). On being the right (cell) size. Science (New York, N.Y.), 348(6236), 1245075. 10.1126/science.1245075 [PubMed: 25977557]

Hannan KM, Brandenburger Y, Jenkins A, Sharkey K, Cavanaugh A, Rothblum L, Moss T, Poortinga G, McArthur GA, Pearson RB, & Hannan RD (2003). mTOR-Dependent Regulation of Ribosomal Gene Transcription Requires S6K1 and Is Mediated by Phosphorylation of the Carboxy-Terminal Activation Domain of the Nucleolar Transcription Factor UBF†. Molecular and Cellular Biology, 23(23), 8862–8877. 10.1128/MCB.23.23.8862-8877.2003 [PubMed: 14612424]

Hashimoto H, Yuasa S, Tabata H, Tohyama S, Hayashiji N, Hattori F, Muraoka N, Egashira T, Okata S, Yae K, Seki T, Nishiyama T, Nakajima K, Sakaue-Sawano A, Miyawaki A, & Fukuda K (2014). Time-lapse imaging of cell cycle dynamics during development in living cardiomyocyte. Journal of Molecular and Cellular Cardiology, 72, 241–249. 10.1016/j.yjmcc.2014.03.020 [PubMed: 24704900]

Hellesvik M, Øye H, & Aksnes H (2020). Exploiting the potential of commercial digital holographic microscopy by combining it with 3D matrix cell culture assays. Scientific Reports, 10(1), 14680. 10.1038/s41598-020-71538-1 [PubMed: 32895419]

Huang H, Huang GN, & Payumo AY (2023). Two decades of heart regeneration research: Cardiomyocyte proliferation and beyond. WIREs Mechanisms of Disease, e1629. 10.1002/wsbm.1629 [PubMed: 37700522]

Leone M, & Engel FB (2019). Pseudo-bipolar spindle formation and cell division in postnatal binucleated cardiomyocytes. Journal of Molecular and Cellular Cardiology, 134, 69–73. 10.1016/j.yjmcc.2019.07.005 [PubMed: 31301302]

Leone M, & Engel FB (2021). Isolation, Culture, and Live-Cell Imaging of Primary Rat Cardiomyocytes. In Poss KD & Kühn B (Eds.), Cardiac Regeneration: Methods and Protocols (pp. 109–124). Springer US. 10.1007/978-1-0716-0668-1_9

Leone M, Magadum A, & Engel FB (2015). Cardiomyocyte proliferation in cardiac development and regeneration: A guide to methodologies and interpretations. American Journal of Physiology. Heart and Circulatory Physiology, 309(8), H1237–1250. 10.1152/ajpheart.00559.2015 [PubMed: 26342071]

Leone M, Musa G, & Engel FB (2018). Cardiomyocyte binucleation is associated with aberrant mitotic microtubule distribution, mislocalization of RhoA and IQGAP3, as well as defective actomyosin ring anchorage and cleavage furrow ingression. Cardiovascular Research, 114(8), 1115–1131. 10.1093/cvr/cvy056 [PubMed: 29522098]

Li F, Wang X, Capasso JM, & Gerdes AM (1996). Rapid transition of cardiac myocytes from hyperplasia to hypertrophy during postnatal development. Journal of Molecular and Cellular Cardiology, 28(8), 1737–1746. 10.1006/jmcc.1996.0163 [PubMed: 8877783]

Mehdipour M, Park S, & Huang GN (2023). Unlocking cardiomyocyte renewal potential for myocardial regeneration therapy. Journal of Molecular and Cellular Cardiology, 177, 9–20. 10.1016/j.yjmcc.2023.02.002 [PubMed: 36801396]

Mohamed TMA, Ang Y-S, Radzinsky E, Zhou P, Huang Y, Elfenbein A, Foley A, Magnitsky S, & Srivastava D (2018). Regulation of Cell Cycle to Stimulate Adult Cardiomyocyte Proliferation and Cardiac Regeneration. Cell, 173(1), 104–116.e12. 10.1016/j.cell.2018.02.014 [PubMed: 29502971]

Mölder A, Sebesta M, Gustafsson M, Gisselson L, Wingren AG, & Alm K (2008). Non-invasive, label-free cell counting and quantitative analysis of adherent cells using digital holography. Journal of Microscopy, 232(2), 240–247. 10.1111/j.1365-2818.2008.02095.x [PubMed: 19017223]

Nakamura M, & Sadoshima J (2018). Mechanisms of physiological and pathological cardiac hypertrophy. Nature Reviews Cardiology, 15(7), Article 7. 10.1038/s41569-018-0007-y

Nakano H, Minami I, Braas D, Pappoe H, Wu X, Sagadevan A, Vergnes L, Fu K, Morselli M, Dunham C, Ding X, Stieg AZ, Gimzewski JK, Pellegrini M, Clark PM, Reue K, Lusis AJ, Ribalet B, Kurdistani SK, … Nakano A (2017). Glucose inhibits cardiac muscle maturation through nucleotide biosynthesis. eLife, 6, e29330. 10.7554/eLife.29330 [PubMed: 29231167]

Porrello ER, Mahmoud AI, Simpson E, Hill JA, Richardson JA, Olson EN, & Sadek HA (2011). Transient Regenerative Potential of the Neonatal Mouse Heart. Science, 331(6020), 1078–1080. [PubMed: 21350179]

Porrello ER, Mahmoud AI, Simpson E, Johnson BA, Grinsfelder D, Canseco D, Mammen PP, Rothermel BA, Olson EN, & Sadek HA (2013). Regulation of neonatal and adult mammalian heart regeneration by the miR-15 family. Proceedings of the National Academy of Sciences of the United States of America, 110(1), 187–192. 10.1073/pnas.1208863110 [PubMed: 23248315]

Ring DB, Johnson KW, Henriksen EJ, Nuss JM, Goff D, Kinnick TR, Ma ST, Reeder JW, Samuels I, Slabiak T, Wagman AS, Hammond M-EW, & Harrison SD (2003). Selective Glycogen Synthase Kinase 3 Inhibitors Potentiate Insulin Activation of Glucose Transport and Utilization In Vitro and In Vivo. Diabetes, 52(3), 588–595. 10.2337/diabetes.52.3.588 [PubMed: 12606497]

Rolfe M, McLeod LE, Pratt PF, & Proud CG (2005). Activation of protein synthesis in cardiomyocytes by the hypertrophic agent phenylephrine requires the activation of ERK and involves phosphorylation of tuberous sclerosis complex 2 (TSC2). The Biochemical Journal, 388(Pt 3), 973–984. 10.1042/BJ20041888 [PubMed: 15757502]

Satoh H, Delbridge LM, Blatter LA, & Bers DM (1996). Surface:volume relationship in cardiac myocytes studied with confocal microscopy and membrane capacitance measurements: Species-dependence and developmental effects. Biophysical Journal, 70(3), 1494–1504. [PubMed: 8785306]

Sen A, Dunnmon P, Henderson SA, Gerard RD, & Chien KR (1988). Terminally differentiated neonatal rat myocardial cells proliferate and maintain specific differentiated functions following expression of SV40 large T antigen. The Journal of Biological Chemistry, 263(35), 19132–19136. [PubMed: 3198615]

Simpson P. (1985). Stimulation of hypertrophy of cultured neonatal rat heart cells through an alpha 1-adrenergic receptor and induction of beating through an alpha 1- and beta 1-adrenergic receptor interaction. Evidence for independent regulation of growth and beating. Circulation Research, 56(6), 884–894. 10.1161/01.res.56.6.884 [PubMed: 2988814]

Singh AP, Umbarkar P, Guo Y, Force T, Gupte M, & Lal H (2019). Inhibition of GSK-3 to induce cardiomyocyte proliferation: A recipe for in situ cardiac regeneration. Cardiovascular Research, 115(1), 20–30. 10.1093/cvr/cvy255 [PubMed: 30321309]

Soonpaa MH, Kim KK, Pajak L, Franklin M, & Field LJ (1996). Cardiomyocyte DNA synthesis and binucleation during murine development. American Journal of Physiology-Heart and Circulatory Physiology. 10.1152/ajpheart.1996.271.5.H2183

Stopp S, Gründl M, Fackler M, Malkmus J, Leone M, Naumann R, Frantz S, Wolf E, von Eyss B, Engel FB, & Gaubatz S (2017). Deletion of Gas2l3 in mice leads to specific defects in cardiomyocyte cytokinesis during development. Proceedings of the National Academy of Sciences of the United States of America, 114(30), 8029–8034. 10.1073/pnas.1703406114 [PubMed: 28698371]

Tahara T, Quan X, Otani R, Takaki Y, & Matoba O (2018). Digital holography and its multidimensional imaging applications: A review. Microscopy (Oxford, England), 67(2), 55–67. 10.1093/jmicro/dfy007 [PubMed: 29471371]

Tseng A-S, Engel FB, & Keating MT (2006). The GSK-3 inhibitor BIO promotes proliferation in mammalian cardiomyocytes. Chemistry & Biology, 13(9), 957–963. 10.1016/j.chembiol.2006.08.004 [PubMed: 16984885]

Wang H, Paulsen MJ, Hironaka CE, Shin HS, Farry JM, Thakore AD, Jung J, Lucian HJ, Eskandari A, Anilkumar S, Wu MA, Cabatu MC, Steele AN, Stapleton LM, Zhu Y, & Woo YJ (2020). Natural Heart Regeneration in a Neonatal Rat Myocardial Infarction Model. Cells, 9(1), 229. 10.3390/cells9010229 [PubMed: 31963369]

Wang S, Ye L, Li M, Liu J, Jiang C, Hong H, Zhu H, & Sun Y (2016). GSK-3β Inhibitor CHIR-99021 Promotes Proliferation Through Upregulating β-Catenin in Neonatal Atrial Human Cardiomyocytes. Journal of Cardiovascular Pharmacology, 68(6), 425–432. 10.1097/FJC.0000000000000429 [PubMed: 27575008]

Wang WE, Li L, Xia X, Fu W, Liao Q, Lan C, Yang D, Chen H, Yue R, Zeng C, Zhou L, Zhou B, Duan DD, Chen X, Houser SR, & Zeng C (2017). Dedifferentiation, Proliferation, and Redifferentiation of Adult Mammalian Cardiomyocytes After Ischemic Injury. Circulation, 136(9), 834–848. 10.1161/CIRCULATIONAHA.116.024307 [PubMed: 28642276]

Watkins SJ, Borthwick GM, Oakenfull R, Robson A, & Arthur HM (2012). Angiotensin II-induced cardiomyocyte hypertrophy in vitro is TAK1-dependent and Smad2/3-independent. Hypertension Research, 35(4), Article 4. 10.1038/hr.2011.196 [PubMed: 22048570]

Windmueller R, Leach JP, Babu A, Zhou S, Morley MP, Wakabayashi A, Petrenko NB, Viatour P, & Morrisey EE (2020). Direct Comparison of Mononucleated and Binucleated Cardiomyocytes Reveals Molecular Mechanisms Underlying Distinct Proliferative Competencies. Cell Reports, 30(9), 3105–3116.e4. 10.1016/j.celrep.2020.02.034 [PubMed: 32130910]

Yahalom-Ronen Y, Rajchman D, Sarig R, Geiger B, & Tzahor E (2015). Reduced matrix rigidity promotes neonatal cardiomyocyte dedifferentiation, proliferation and clonal expansion. eLife, 4, e07455. 10.7554/eLife.07455 [PubMed: 26267307]

Zak R. (1973). Cell proliferation during cardiac growth. The American Journal of Cardiology, 31(2), 211–219. 10.1016/0002-9149(73)91034-5 [PubMed: 4265520]

Zatulovskiy E, Zhang S, Berenson DF, Topacio BR, & Skotheim JM (2020). Cell growth dilutes the cell cycle inhibitor Rb to trigger cell division. Science (New York, N.Y.), 369(6502), 466–471. 10.1126/science.aaz6213 [PubMed: 32703881]

Zhang Y, & Judson RL (2018). Evaluation of holographic imaging cytometer holomonitor M4® motility applications. Cytometry. Part A: The Journal of the International Society for Analytical Cytology, 93(11), 1125–1131. 10.1002/cyto.a.23635 [PubMed: 30343513]

Zhou J, Ahmad F, Parikh S, Hoffman NE, Rajan S, Verma VK, Song J, Yuan A, Shanmughapriya S, Guo Y, Gao E, Koch W, Woodgett JR, Muniswamy M, Kishore R, Lal H, & Force T (2016). Loss of Adult Cardiac Myocyte GSK-3 Leads to Mitotic Catastrophe Resulting in Fatal Dilated Cardiomyopathy. Circulation Research, 118(8), 1208–1222. 10.1161/CIRCRESAHA.116.308544 [PubMed: 26976650]

HIGHLIGHTS

- Digital holographic imaging enables quantitative label-free monitoring of primary cardiac cultures *in vitro*
- Primary cardiomyocytes can be readily distinguished from non-cardiomyocytes based on their larger size and slower motility
- Mononucleated and binucleated cardiomyocytes reach a similar relative size-increase threshold prior to cell division

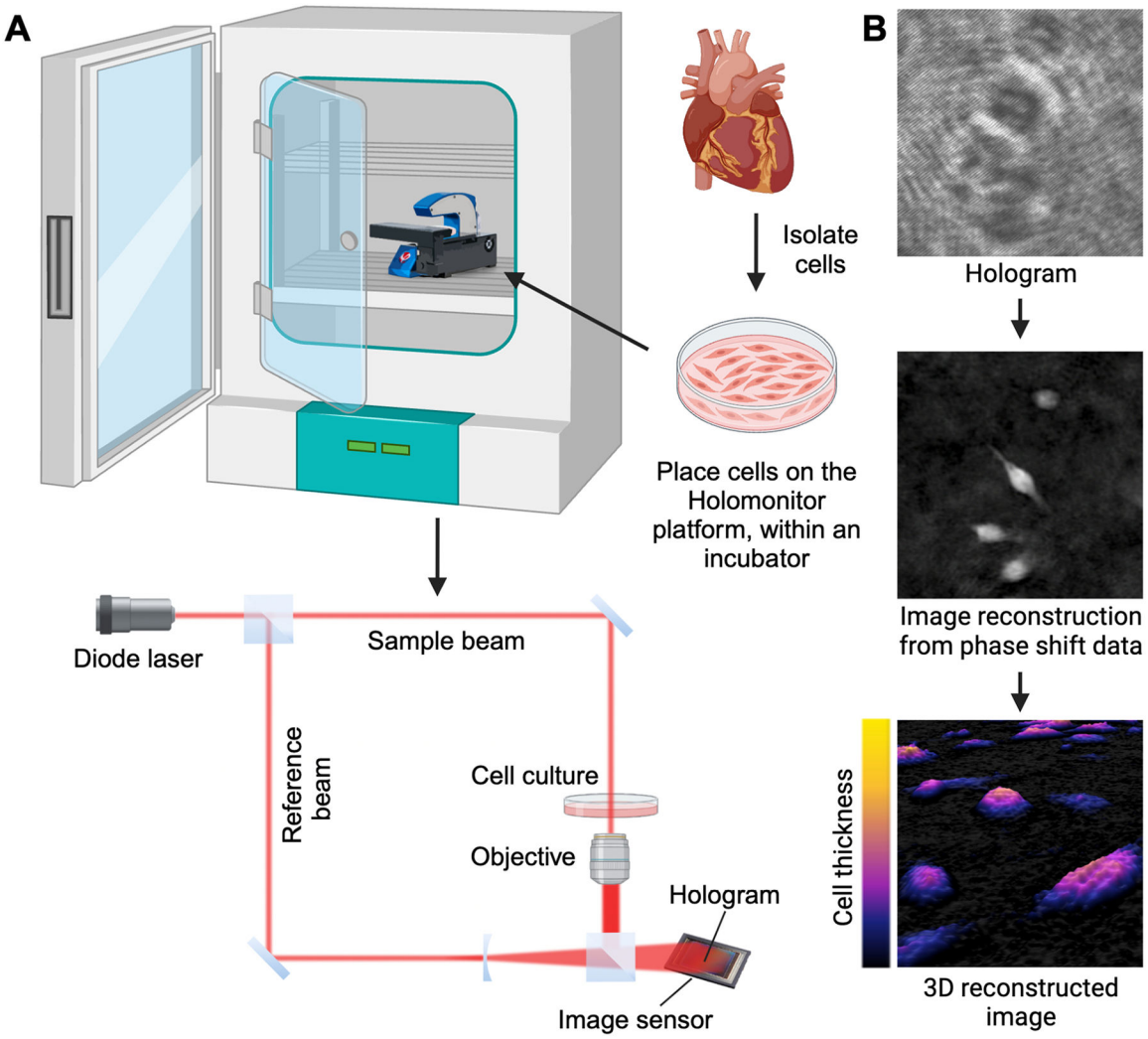

Figure 1: Three-dimensional digital holographic imaging of cultured primary cardiac cells with the Holomonitor M4.

(**A**) Primary cardiac cultures are placed onto the Holomonitor M4 housed within a standard CO_2 incubator. A diode laser is divided into a reference beam and an object beam that passes through the sample, which creates a phase shift. An interference pattern hologram is generated by merging of the object and reference beams. This is recorded by an image sensor to reconstruct a phase image. (**B**) Example images of an interference pattern hologram and three-dimensional reconstructions of cultured primary rat cardiomyocytes as visualized on the Holomonitor M4. Created with BioRender.com.

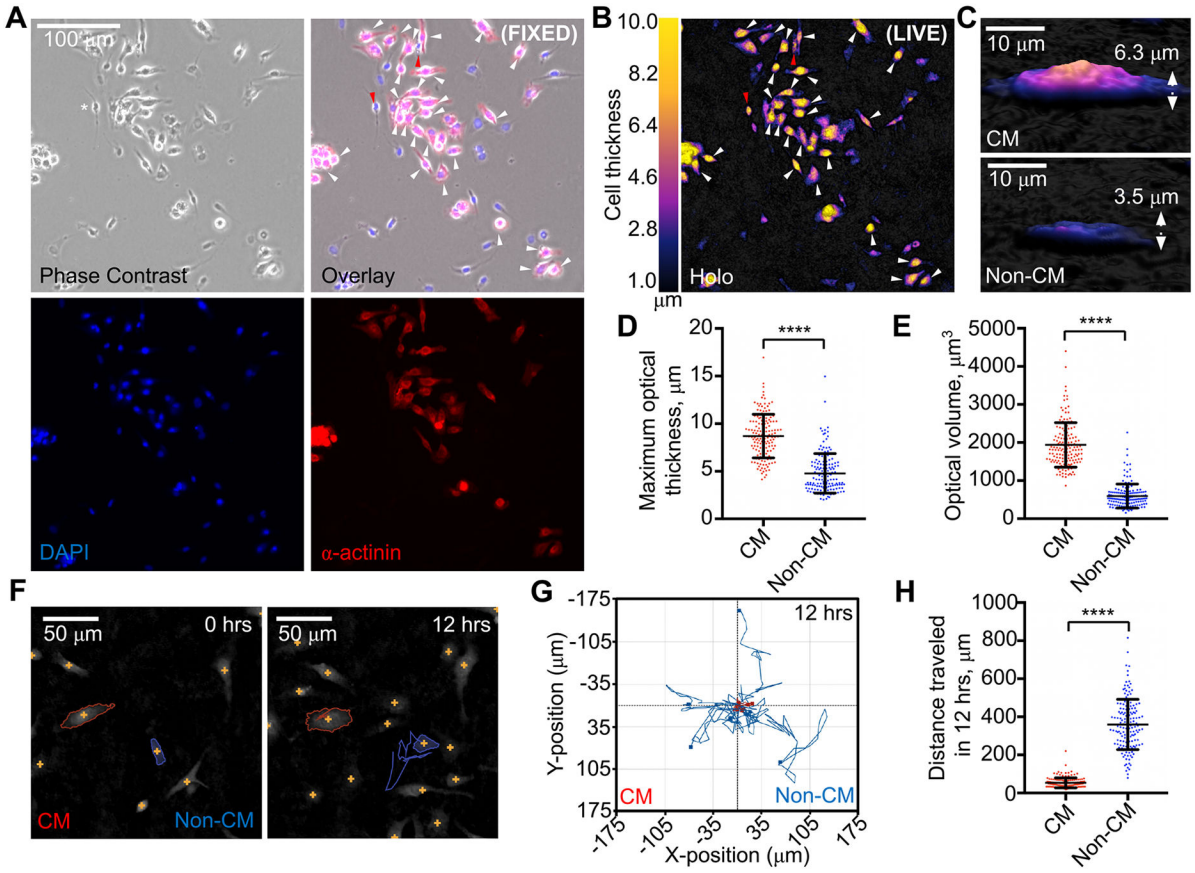

Figure 2: Label-free digital holographic microscopy identifies primary rat cardiomyocytes based on their larger size and limited motility.

(**A-B**) The same imaging field of fixed postnatal day 2 (P2) rat cardiac cells visualized on a phase contrast fluorescence microscope (**A**) or live on the Holomonitor M4 (**B**). Arrowheads (28 total) indicate putative cardiomyocytes based on larger cell size alone. Those with white arrowheads (26/28) are correctly identified as α-actinin-positive cardiomyocytes. Those with red arrowheads (2/28) are incorrectly identified. DAPI labels all nuclei. The imaging magnification in **A** and **B** are conserved. (**C-E**) Representative three-dimensional reconstructions of a CM and non-CM (**C**) and quantifications of their maximum optical thicknesses (**D**) and optical volumes (**E**). (**F-H**) Motility analysis of CMs and non-CMs. (**F**) Representative segmentation and tracking of a CM (red outline) and non-CM (blue outline) over 12 hours. Cell trajectories are shown as a single solid line for each cell. (**G**) Overlayed trajectories of CMs (n=7) and non-CMs (n=7) over 12 hours. All cell traces begin at the (0,0) coordinate. (**H**) Total distance traveled by each cell over 12 hours. 150 CMs and 151 non-CMs from postnatal day 2 (P2) hearts across 3 independent isolations were analyzed in **D, E**, and **H**. Values are reported as mean ± standard deviation. Student's t-test; ****, $P < 0.0001$.

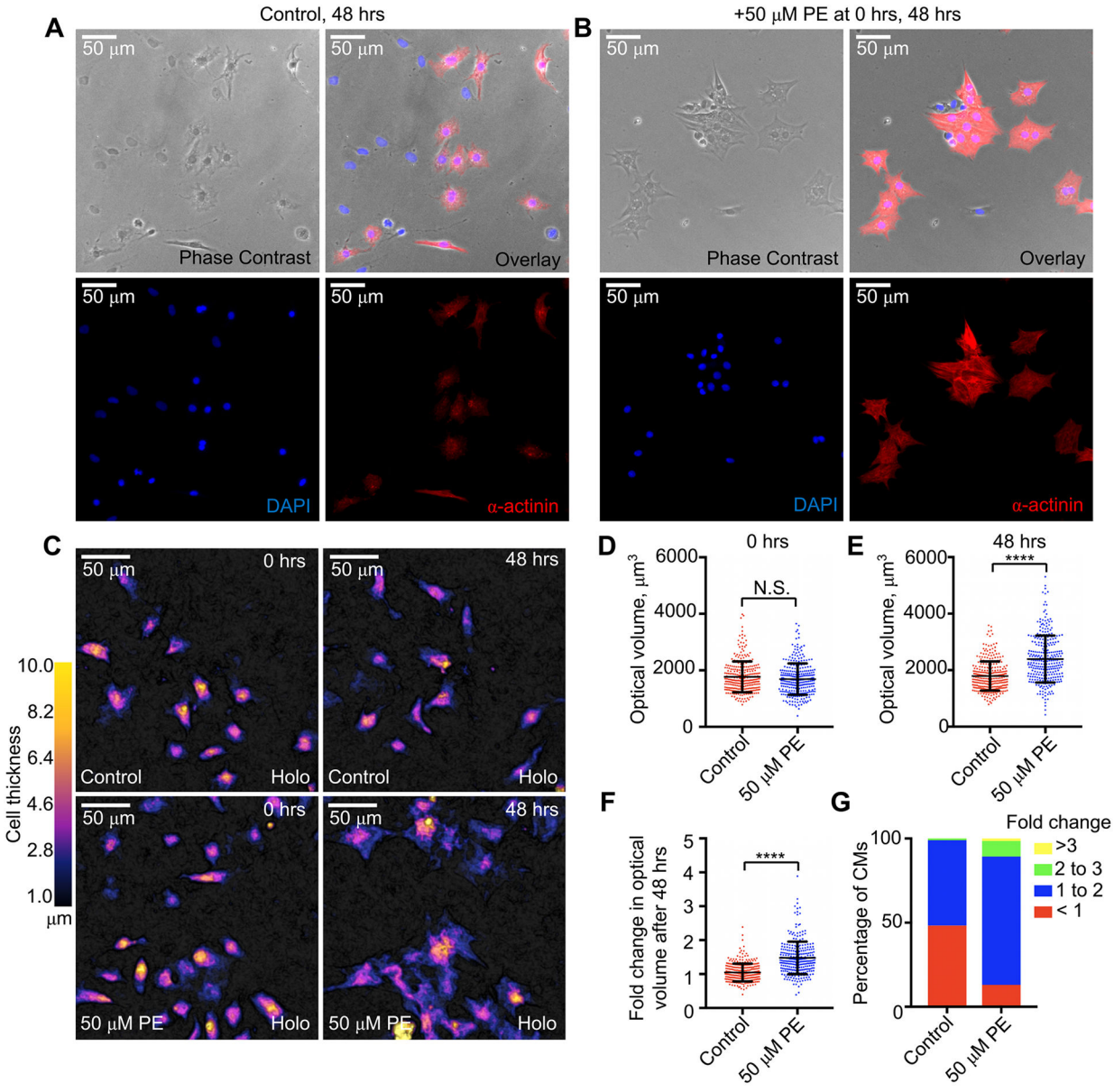

Figure 3: Digital holographic imaging of cardiomyocyte volume dynamics in response to a hypertrophic stimulus.

(**A-B**) Phase-contrast and fluorescence micrographs of primary rat cardiomyocytes (CM) untreated (**A**) or treated with 50 μM phenylephrine (PE; **B**) for 48 hours. Cardiac cultures were stained for the CM-specific marker α-actinin and DAPI to label all nuclei. (**C-G**) Representative digital holographic images of untreated CMs or those treated with 50 μM PE for 48 hours (**C**). (**D-G**) Quantification of CM raw optical volumes at 0 hours (**D**) and 48 hours (**E**). Fold change in CM optical volumes observed after 48 hours (**F**). Percentage of CMs that exhibit fold changes in volume within specified bins (**G**). 305 untreated and 300 treated cardiomyocytes across 6 independent isolations from postnatal day 1 (P1) and P2 hearts were analyzed. Values are reported as mean ± standard deviation. Student's t-test; ****, $P < 0.0001$; N.S., not significant.

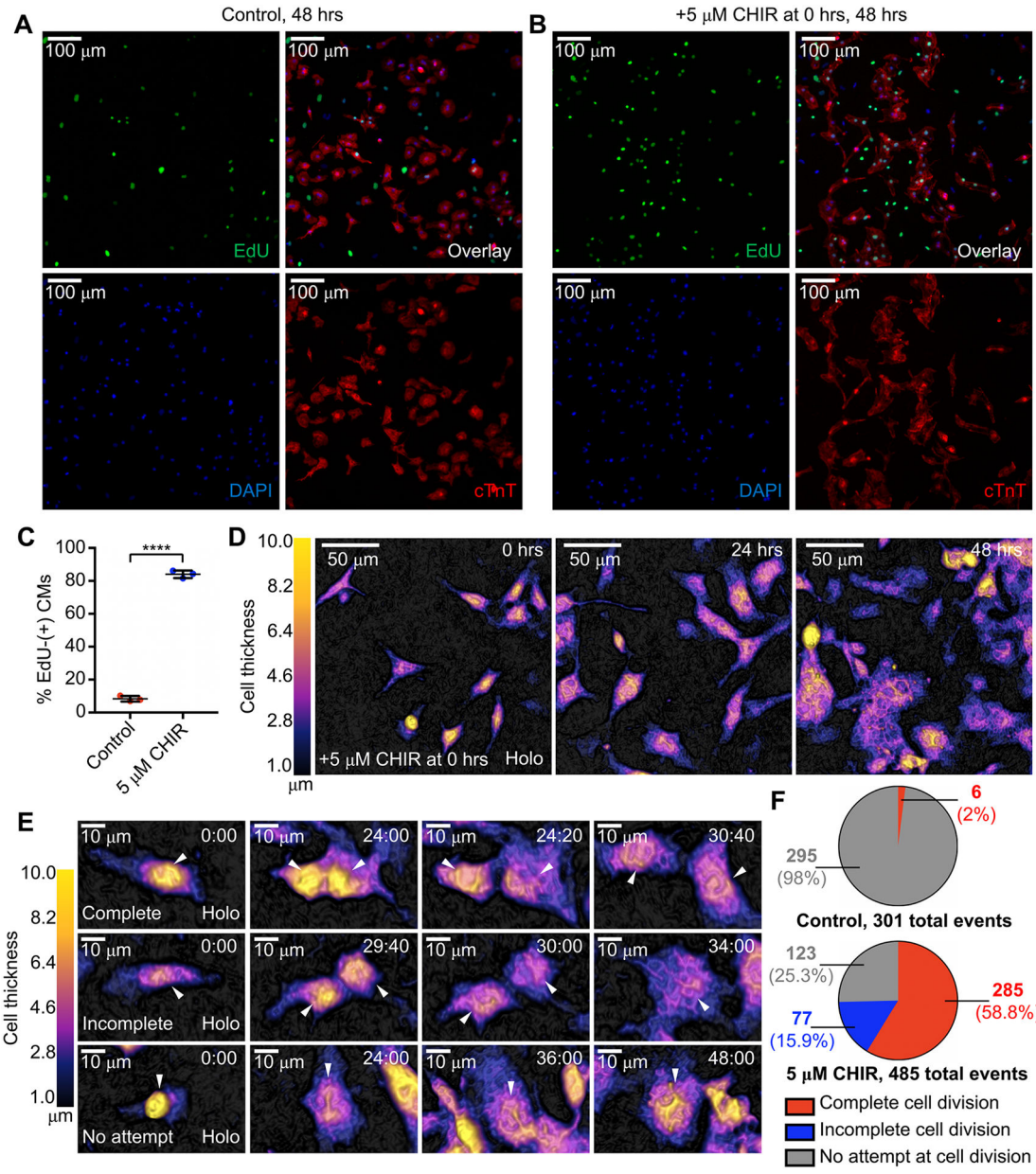

Figure 4: Digital holographic imaging distinguishes between complete and incomplete cardiomyocyte cell division.

(**A**-**C**) Representative fluorescence micrographs of postnatal day 1 (P1) rat cardiomyocytes (CM) untreated (**A**) or treated with 5 μM CHIR99021, a Gsk3β inhibitor (**B**) for 48 hours. Cultures were stained for CM-specific marker cardiac Troponin T (cTnT) and DAPI to label all nuclei. Cells incorporating ethynyl-2'-deoxyuridine (EdU), an S-phase marker, after 48-hour incubation were identified. Quantification of EdU- and cTnT-double positive cells from three independent cultures (**C**). (**D**) Representative digital holographic images of P3 CMs stimulated with 5 μM CHIR99021 at 0 h, 24 h, and 48 hrs post-treatment. (**E**-**F**) Representative digital holographic time-lapse images showing examples of CMs that complete, incomplete, or make no attempts at cell division post stimulation (time stamp, hours:minutes) (**E**) and outcome analysis of 301 DMSO control-treated and 485

CHIR99021-treated cardiomyocytes across 3 and 4 independent isolations from postnatal day 3 (P3) and P3-P4 hearts, respectively (**F**). Values are reported as mean ± standard deviation. Student's t-test; ****, $P < 0.0001$.

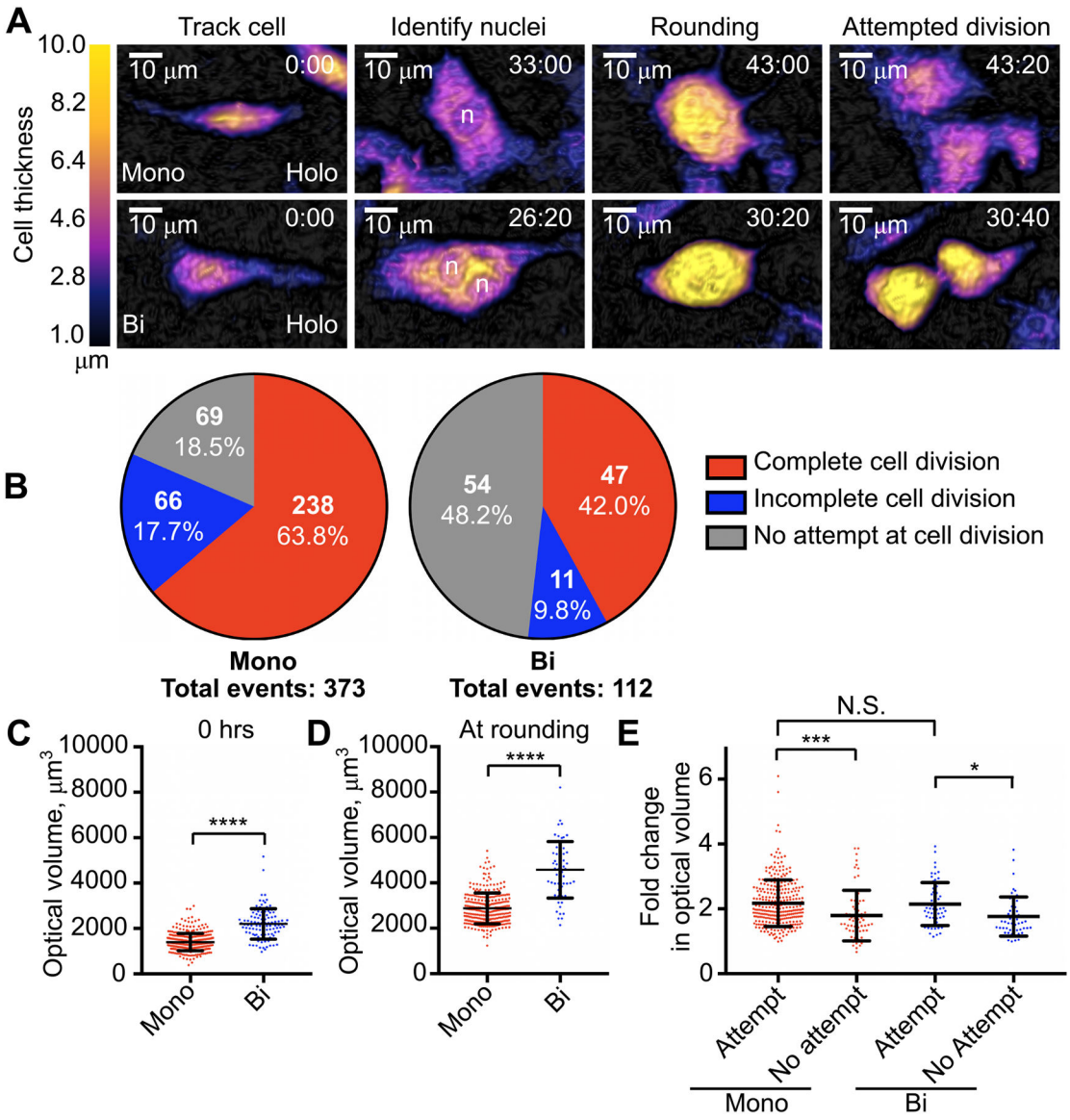

Figure 5: Binucleation blunts cardiomyocyte responses to a proliferative stimulus.

(**A**) Representative digital holographic time-lapse images of postnatal day 3 (P3) cardiomyocytes (CMs) stimulated to divide with 5 μM CHIR99021 (timestamp, hours:minutes). Example nuclei identified to distinguish mononucleated from binucleated CMs are marked with "n". (**B**) Outcome analyses of all 373 mononucleated and 112 binucleated CMs analyzed. (**C-D**) Optical volumes of all mononucleated and binucleated CMs in **B** at 0 hours (**C**), and the time of rounding (n = 304 and n = 58, respectively) (**D**). Fold change in optical volumes observed at rounding for mononucleated and binucleated CMs that attempt to divide (n = 304 and n = 58, respectively) or by 48 hours for mononucleated and binucleated CMs that make no attempt at cell division (n = 69 and n = 54, respectively) (**E**). Values are reported as mean ± standard deviation. Cells measurements compiled from postnatal day 3 (P3) hearts across 4 independent isolations (**C-D**) Student's

t-test; ****, P < 0.0001. (**E**) One-way ANOVA, Tukey's multiple comparisons test; ***, P < 0.001; *, P < 0.05; N.S., not significant.